Cell Mol Neurobiol (2014) 34:951–961
DOI 10.1007/s10571-014-0081-6

REVIEW PAPER

Upregulated Expression of SSTR1 is Involved in Neuronal Apoptosis and is Coupled to the Reduction of bcl-2 Following Intracerebral Hemorrhage in Adult Rats

Damin Yuan · Jianhong Shen · Yaohua Yan · Xinmin Wu · Aihong Li · Aisong Guo · Yuanyuan Wu · Chengwei Duan · Jiabing Shen · Cuiying Tang · Dongmei Zhang · Yuhong Ji

Received: 15 April 2014 / Accepted: 29 June 2014 / Published online: 18 July 2014

Abstract Somatostatins are peptide hormones that regulate diverse cellular processes, such as neurotransmission, cell proliferation, apoptosis, and endocrine signaling as well as inhibiting the release of many hormones and other secretory proteins. SSTR1 is a member of the superfamily of somatostatin receptors possessing seven-transmembrane segments. Aberrant expression of SSTR1 has been implicated in several human diseases, including pseudotumor cerebri, and oncogenic osteomalacia. In this study, we investigated a potential role of SSTR1 in the regulation of neuronal apoptosis in the course of intracerebral hemorrhage (ICH). A rat ICH model in the caudate putamen was established and subjected to behavioral tests. Western blot and immunohistochemistry indicated a remarkable up-regulation of SSTR1 expression surrounding the hematoma after ICH. Double-labeled immunofluorescence showed that SSTR1 was mostly co-localized with neurons, and was rarely distributed in activated astrocytes and microglia. Additionally, SSTR1 co-localized with active-caspase-3 and bcl-2 around the hematoma. The expression of active-caspase-3 was parallel with that of SSTR1 in a time-dependent manner. In addition, SSTR1 knockdown specifically resulted in reduced neuronal apoptosis in PC12 cells. All our findings suggested that up-regulated SSTR1 contributed to neuronal apoptosis after ICH, which was accompanied with reduced expression of bcl-2.

Keywords Intracerebral hemorrhage · SSTR1 · Neuron · Apoptosis

Damin Yuan and Janhong Shen contributed equally to this work.

D. Yuan · Y. Ji (✉)
Jiangsu Province Key Laboratory for Inflammation and Molecular Drug Target, Department of Immunology, Medical College, Nantong University, Nantong 226001, People's Republic of China
e-mail: yuandamin99@163.com

J. Shen · Y. Yan · X. Wu · A. Li · A. Guo · Y. Wu
Department of Neurosurgery, Affiliated Hospital of Nantong University, Nantong, Jiangsu Province, People's Republic of China

C. Duan
Jiangsu Key Laboratory of Neuroregeneration, Nantong University, Nantong 226001, People's Republic of China

J. Shen
Department of Neurology, Affiliated Hospital of Nantong University, Nantong, Jiangsu Province, People's Republic of China

C. Tang
Department of Nutrition and Food Hygiene, School of Public Health, Nantong University, Nantong 226001, Jiangsu Province, People's Republic of China

D. Zhang (✉)
Jiangsu Province Key Laboratory for Inflammation and Molecular Drug Target, Department of Pathogen Biology, Medical College, Nantong University, Nantong 226001, People's Republic of China
e-mail: zdm@ntu.edu.cn

Introduction

ICH is a particularly deadly type of stroke affecting 2 million people worldwide each year (Qureshi et al. 2009). Compared with white populations, Chinese populations have been reported to have a higher proportion of ICH (Tsai et al. 2013). ICH is an acute and spontaneous process when a weakened blood vessel ruptures and the blood flows into the brain parenchyma, especially the ventricles and the subarachnoid space (Aronowski and Zhao 2011). Compared with ischemia stroke, ICH has a higher incidence of major disability and death. Although a lot of resources have been thrown into clinical and basic researches on ICH, the prognosis of patients remains very poor (Ikram et al. 2012). To figure out the clinical outcome of ICH, investigation into the pathogenesis of ICH-induced brain injury is a main task. ICH causes primary injury through physical disruption of adjacent tissue and the mass effect. Along with primary injury, secondary injury might occur, caused by factors such as brain edema, inflammation, and oxidative stress (Rui et al. 2013). Pathologic changes of ICH include neuronal apoptosis, astrocyte proliferation, and oligodendrocyte death (Bradl and Lassmann 2010; Karwacki et al. 2005; Wang and Dore 2007). Among them, neuronal apoptosis is considered to be one of the most crucial events, whose decision depends on complex pro-apoptotic and subtle anti-apoptotic modulation (Li et al. 2013). Apoptosis, also known as programmed cell death, is a form of cell death that constitutes part of a common mechanism in cell replacement, tissue remodeling, and the removal of damaged cells (Yoon et al. 2013). Apoptosis can be triggered by extrinsic pathway and intrinsic pathway. The former is initiated by ligation of death receptors, the recruitment and activation of caspase-8 at the receptor complexes, while the latter is mitochondria-dependent mechanism, associated with the release of cytochrome c and activation of caspase-9 (Liu et al. 1996). Meanwhile, caspase-3 is a main executioner caspase and can be usually activated by both pathways. Caspase-3 activation by pro-apoptotic bcl-2-family protein Bax has been found to be a decisive factor in p53-induced apoptosis in neurons (Cregan et al. 1999). Although multiple researches have focused on the mechanisms underlying ICH, current knowledge with the molecular and cellular mechanisms remains much elusive, and much more work should be done to identify novel strategies in the further treatment of ICH.

Somatostatin receptors (SSTRs) are seven-transmembrane guanosine triphosphate-binding protein-coupled membrane receptors (GPCRs) that belong to the G-protein-coupled receptor family (Patel and Srikant 1994; Watt et al. 2009). SSTRs are present in somatostatin (SST) target tissues, such as brain, pituitary, pancreas, and gastrointestinal tract (Chatterjee et al. 2007; Reubi 1992). SST, a regulatory peptide with two bioactive forms, SST-14 and SST-28, is generated in neuroendocrine cells in the brain and periphery and acts on a mass of tissue targets to modulate neurotransmission, cell secretion, and cell proliferation (Epelbaum et al. 1994; Patel 1999). The widespread distribution of SST and its receptors indicate that they exert multiple biological functions. SST also inhibits cell proliferation and promotes apoptosis through binding to specific cell-surface SSTRs. The various effects of SST are mediated by specific, high-affinity membrane bound SSTRs on target tissues. Heretofore, five subtypes of SSTRs, SSTR1, -2, -3, -4, and -5, have been identified (Akopian et al. 2000). In some cells, the activation of SSTR subtypes not only directly inhibits their proliferation but is also relevant to the initiation of apoptosis (Sharma et al. 1996; Sharma and Srikant 1998; Teijeiro et al. 2002). SSTR2 and SSTR3 are the most important receptor subtypes mediating growth hormone secretion, endothelial cell cycle arrest, and retinal endothelial cell apoptosis (Hu et al. 2004). Studies demonstrated that activation of SSTR2 promotes apoptosis in HL-60 cells. What is more, in contrast with the proapoptotic mechanism previously reported for SSTR3, cell death induced by activation of SSTR2 is independent from accumulation of p53 (Teijeiro et al. 2002). Coexpression of human somatostatin receptor-2 (SSTR2) and SSTR3 modulates antiproliferative signaling and apoptosis in HEK-293 cells (War and Kumar 2012). Also, SSTR1, SSTR2, SSTR3, and SSTR5 subtypes can influence the apoptosis of tumor cells and affect the progression of colorectal cancer by down-regulating the bcl-2 expression or resisting the anti-apoptotic effect of bcl-2 (Qiu et al. 2006; Teijeiro et al. 2002). bcl-2 family proteins are divided into three groups on the basis of their proapoptotic (e.g. Bax, Bak) or anti-apoptotic action (e.g. bcl-2, bcl-xL) and the bcl-2 Homology (BH) domains they possess. In the pancreatic tumor mouse models overexpression of SSTR2 could lead to decreased level of bcl-2 protein and cell apoptosis in pancreatic tumor cells. (Rochaix et al. 1999). These findings promote us to question whether SSTR1 has some relationship with apoptosis as a member of the SSTR family. It has been reported that SSTR1 could facilitate apoptosis via the blockage of G1/S progression in the cell cycle (Stetak et al. 2001). As five SSTR subtypes are all related to apoptosis, whether they take part in the pathophysiologic processes following ICH remains to be investigated.

We hereby conjecture that SSTR1 might be involved in the secondary damage following ICH. To test this hypothesis, we examined the expression and distribution of SSTR1 surrounding the hematoma in an ICH rat model. The colocalizations of SSTR1 and active caspase-3/bcl-2 were also detected. These data together indicate that SSTR1 might take part in the neuronal apoptosis after ICH.

Animals and the ICH Model

All animal care and surgical procedures were performed in accordance with the National Institutes of Health Guidelines for the Care and Use of Laboratory Animals (National Research Council, 1996, USA); all animal protocols were sanctioned by the Chinese National Committee to the Use of Experimental Animals for Medical Purposes, Jiangsu Branch. Adult male Sprague–Dawley rats with an average weight of 250 g were used in this study. The rats were anesthetized intraperitoneally with chloral hydrate (10 % solution) and then positioned in a stereotaxic frame, and a cranial burr hole (1 mm in diameter) was drilled. Autologous whole blood (50 μL) was collected in a sterile syringe by cutting the tail tip (Xue and Del Bigio 2003). The sterile syringe was inserted stereotaxically into the right caudate putamen (coordinates: 0.2 mm anterior, 5.5 mm ventral, and 3.5 mm lateral to the bregma) (Hua et al. 2002). The sham-operated group only had a needle insertion. The needle was kept in place for over 10 min before removed, the skin incision closed, animals were allowed to under a 12 h light/dark cycle in a pathogen-free condition. Experimental animals ($n = 6$–8 per time point) were sacrificed to extract the protein for Western blot analysis at 3 and 6h, 12 h, 1, 2, 3, 5, and 7 day(s) ($n = 3$ per time point) following ICH, respectively. The sham group ($n = 6$–8 per time point) was sacrificed on the second day. Additional two rats at each time point from the experimental group were killed for pathologic studies. All efforts have been made to minimize the number of animals used and their suffering.

Cell Cultures and Stimulation

PC12 cells were cultured in Dulbecco's modified Eagle's medium with 10 % (v/v) fetal bovine serum, 5 % donor horse serum, and 1 % antibiotics (penicillin) at 37 °C under 5 % CO2 in humidified air. The cells were passaged every 3–4 days. In order to study apoptosis, PC12 cells were seeded onto a poly-L-lysine-coated 60 mm dishes and incubated in a low concentration of serum (1 % horse serum) for 24 h prior to treatment with hemin in 100 μmol/L at various time points.

Behavioral Testing Procedures

Forelimb Placing Test

Rats were held by the torsos, keeping the forelimb to hang free. Each forelimb was elicited by brushing the respective vibrissae on the corner edge of a countertop. Intact rats put the forelimb quickly onto the countertop. According to the extent of injury, placing of the forelimb contralateral to the injury was impaired. During the experiments, each rat was tested 10 times for each forelimb, and the percentage of trials in which the rat placed the left forelimb was calculated (Karabiyikoglu et al. 2004).

Corner Turn Test

The rats were allowed to proceed into a corner, with the angle of 30. To exit the corner, the rat should turn either to the left or to the right, and only the turns involving full rearing along either wall were involved (a total of eight per animal). Based on the extent of injury, rats may show a tendency to turn to the side of the injury. The percentage of right turns was used as the corner turn score. And the animals were not picked up immediately after each turn so that they would not appear an aversion for their prepotent turning response (Huan et al. 2012).

Western Blot Analysis

Rats were executed at different time points after operation once given an overdose of chloral hydrate. The caudate putamen tissues surrounding the hematoma (2 mm from the incision) as well as the equal part of the contralateral or sham group were excised and instantly frozen at −80 °C until use. In order to prepare lysates, frozen brain tissue samples were minced with eye scissors in ice. The samples were then homogenized in lysis buffer (1 % NP-40, 50 mmol/l Tris, pH = 7.5, 5 mmol/l EDTA, 1 % SDS, 1 % sodium deoxycholate, 1 % Triton X-100, 1 mmol/l PMSF, 101 g/ml aprotinin, 11 g/ml leupeptin) and clarified by centrifuging for 20 min in a microcentrifuge at 4 °C. After the determination of concentration with the Bradford assay (Bio-Rad), the samples were subjected to SDS–polyacrylamide gel electrophoresis and transferred to a polyvinylidene difluoride (PVDF) filter membrane by a transfer apparatus at 350 mA for 2 h. The membrane was then blocked with 5 % nonfat milk and incubated with primary antibody against SSTR1 (anti-rabbit, 1:2,000; Santa Cruz), active caspase-3 (anti-mouse, 1:500; Cell Signaling), bcl-2 (anti-mouse, 1:500; Santa Cruz), GAPDH (anti-rabbit, 1:1,000; Sigma) at 4 °C overnight. After incubating with horseradish peroxidase-conjugated secondary antibody for 2 h, protein was visualized using an enhanced chemiluminescence system (ECL, Pierce Company, USA).

Immunohistochemistry

After defined survival times (2 days following ICH), rats ($n = 3$ for each time point) were terminally anesthetized and perfused through the ascending aorta with 500 ml of 0.9 % saline, followed by 4 % paraformaldehyde. After perfusion, the brains were removed and postfixed in the same fixative overnight and then replaced with 20 %

sucrose solution for 2–3 days, following 30 % sucrose solution for 2–3 days. Tissues were then cut at 7 μm with a cryostat and processed for immunohistochemistry analysis. Sections were kept in an oven at 37 °C for 30 min, and rinsed twice in 0.01 M PBS for 5 min. The sections were processed in 10 mmol/L citrate buffer (pH = 6.0) and heated to 121 °C in an autoclave for 3 min to retrieve the antigen. The sections were taken from the pressure cooker and cooled to room temperature naturally. After rinsing in PBS, all sections were pre-incubated in a solution consisting of 10 % donkey serum, 1 % bovine serum album in (BSA), 0.3 % Triton X-100, and 0.15 % Tween-20 for 2 h at room temperature and incubated with anti- SSTR1 (rabbit, 1:100, Santa Cruz) overnight at 4 °C. Following this, biotinylated secondary antibody (Vector Laboratories, Burlingame, CA) was also incubated for 2 h at room temperature. Staining was visualized with 0.02 % diaminobenzidine tetrahydrochloride (DAB; Vector Laboratories). Finally, the sections were dehydrated, cleared, and covered with cover slips. The sections were observed at ×20, or ×40 magnifications on a Leica light microscope (Germany). We examined the sections and counted the cells with strong or moderate brown staining, weak, or no staining as positive or negative SSTR1 cells, respectively, from each group at higher magnification. We took the average assays of each group as the valuable results.

Double Immunofluorescent Labeling

After air-dried for 1 h at room temperature, sections were blocked with 10 % normal serum blocking solution-species the same as the secondary antibody, containing 3 % (w/v) bovine serum albumin (BSA) and 0.1 % Triton X-100 and 0.05 % Tween-20 2 h at room temperature to avoid unspecific staining. Then, the sections were incubated with primary antibodies against SSTR1 (rabbit; 1:100), NeuN (mouse; 1:500; Chemicon), GFAP (mouse; 1:200; Sigma), CD11b (mouse; 1:50; Serotec), active caspase-3 (mouse or rabbit; 1:200; Santa Cruz), and bcl-2 (anti-mouse, 1:100; Santa Cruz). Briefly, sections were incubated with both primary antibodies overnight at 4 °C, followed by a mixture of FITC- and TRITC-conjugated secondary antibodies (Jackson ImmunoResearch) for 2 h at 4 °C. In order to detect the morphology of the nucleus, sections were stained with DAPI (0.1 mg/mL in PBS; Sigma) for 40 min at 30 °C. The stained sections were examined with a Leica fluorescence microscope (Germany).

SSTR1 siRNA and Transfection

Primer pairs for the SSTR1 (NM_001049) siRNA expression vector targeted the sequence of 5′ ACCAACATCTACA TCCTAA3′. For transient transfection, the SSTR1 siRNA vector or the non-specific vector was carried out using lipofectamine 2,000 (Invitrogen) and plus reagent in OptiMEM (Invitrogen) as suggested by the manufacturer. Transfected cells were cultured for 48 h before use.

Exclusions and Mortality

Three animals in Western blot, four in immunohistochemistry, and six in immunofluorescent were excluded due to technical difficulties, experimenter error, and mortality. Mortality occurred only after the operation error to cause severe ICH. In total, nine animals had a severe ICH, four of which died within 24 h ($p = 0.215$ vs. SHAM). Three died quickly after ICH. After exclusions, twelve rats remained (ICH: $n = 6$, SHAM: $n = 6$), immunohistochemistry had twelve rats (ICH: $n = 6$, SHAM: $n = 6$), and immunofluorescent had 16 rats (ICH: $n = 8$, SHAM: $n = 8$).

Quantitative Analysis

Cell quantification was performed in an unbiased manner. To avoid counting the same cells in adjacent sections, we counted every fifth section (50 μm a part). To identify the proportion of each phenotype-specific marker-positive cells expressing SSTR1, a minimum of 200 phenotype-specific marker-positive cells were counted 3 mm surrounding the hematoma in each section. The number of cells double-labeled for SSTR1 and NeuN, GFAP, or CD11b was also quantified. Two or three intermittent sections (50 μm apart) per animal sections per animal were sampled.

Statistical Analysis

All data were analyzed with Stata 7.0 statistical software. All values were expressed as mean ± standard error of mean (SEM). The statistical significance of differences between groups was determined by one-way analysis of variance followed by Tukey's post hoc multiple comparison tests. $p < 0.05$ or $p < 0.01$ was considered significant. Each experiment consisted of at least three replicates per condition.

Results

The Establishment of ICH Animal Model and the Expression Profiles of SSTR1 After ICH by Western Blot Analysis

In order to reduce mortality, here we chose to induce ICH in the caudate putamen. ICH animal model was established

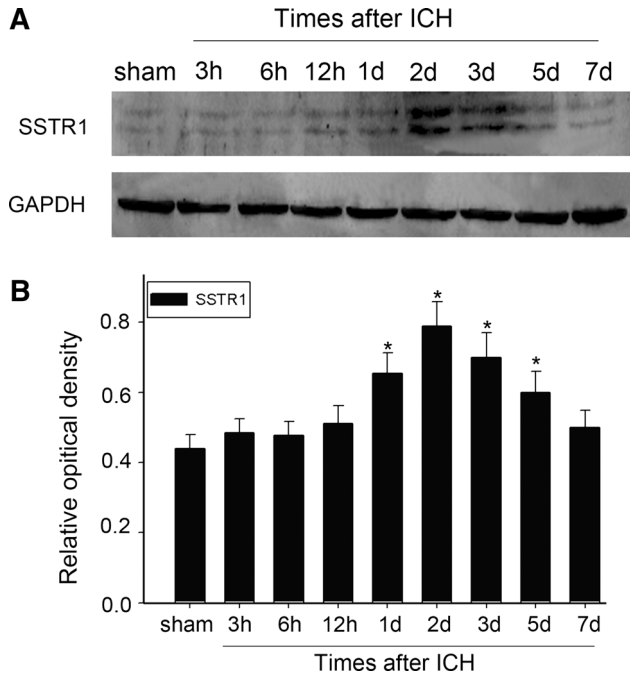

Fig. 1 The expression pattern of SSTR1 following ICH. Western blot analysis was performed to determine the protein level of SSTR1 in ipsilateral caudate putamen around the hematoma at different time periods after ICH. SSTR1 protein level was comparatively low in the sham brain, then increased gradually after ICH, peaked at day 2 and reduced subsequently (**a**). Quantification graphs (relative optical density) of the intensity of staining of SSTR1 to GAPDH at each time point. GAPDH was used as loading control. The data are mean ± SEM (**b**). ($n = 3$, $^*p < 0.05$, significantly distinct from the sham group)

in our previous studies (Liu et al. 2014). Western blot was used to investigate the temporal pattern of SSTR1 expression surrounding the hematoma at different time points. SSTR1 protein level was relatively lower in the sham-control group, whereas it increased at 12 h, reached a peak at day 2, and gradually decreased thereafter in the perihematomal region (Fig. 1a, b).

Changes in the Expression and Distribution of SSTR1 Immunoreactivity

Immunohistochemistry was applied to determine the distribution of SSTR1 at 2 days following ICH. As shown in Fig. 2, the immunostaining signal of SSTR1 was dramatically increased in the brain tissue surrounding the hematoma at day 2 after ICH (Fig. 2e, f, h). Consistent with the results from Western blot, the sham group showed low level of SSTR1 staining (Fig. 2a, b), which was comparable with the expression profile of SSTR1 in the contralateral side of the experimental brains (Fig. 2c, d). No staining was observed in the negative control (Fig. 2g).

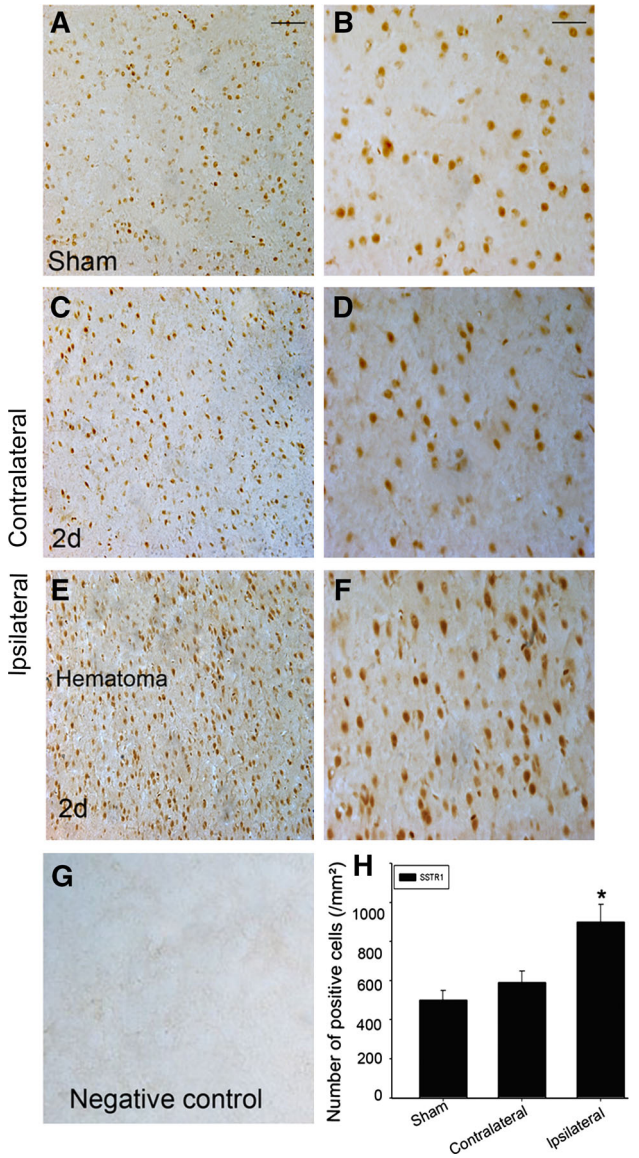

Fig. 2 Immunohistochemistry analysis of the distribution changes of SSTR1in the perihematomal region after ICH. Low level of SSTR1 was detected in the sham group (**a**, **b**). At day 2 after ICH, the contralateral group showed no significant difference in SSTR1 expression (**c**, **d**), while the ipsilateral group expression, compared with the sham group (**e**, **f**) showed increased SSTR1 (**e**, **f**). No positive signals were found in the negative control (**g**). The number of SSTR1-positive cells was significantly increased in the ipsilateral group compared with the sham and contralateral groups (H). * $p < 0.05$. *Scale bar left column* 50 μm; *right columns* 10 μm

Co-localization of SSTR1 with Different Cellular Markers in the Rat Caudate Putamen Around the Hematoma After ICH by Double Immunofluorescent Staining

To further identify which cell types may be associated with the peak expression of SSTR1 after ICH (Fig. 3a, f, k),

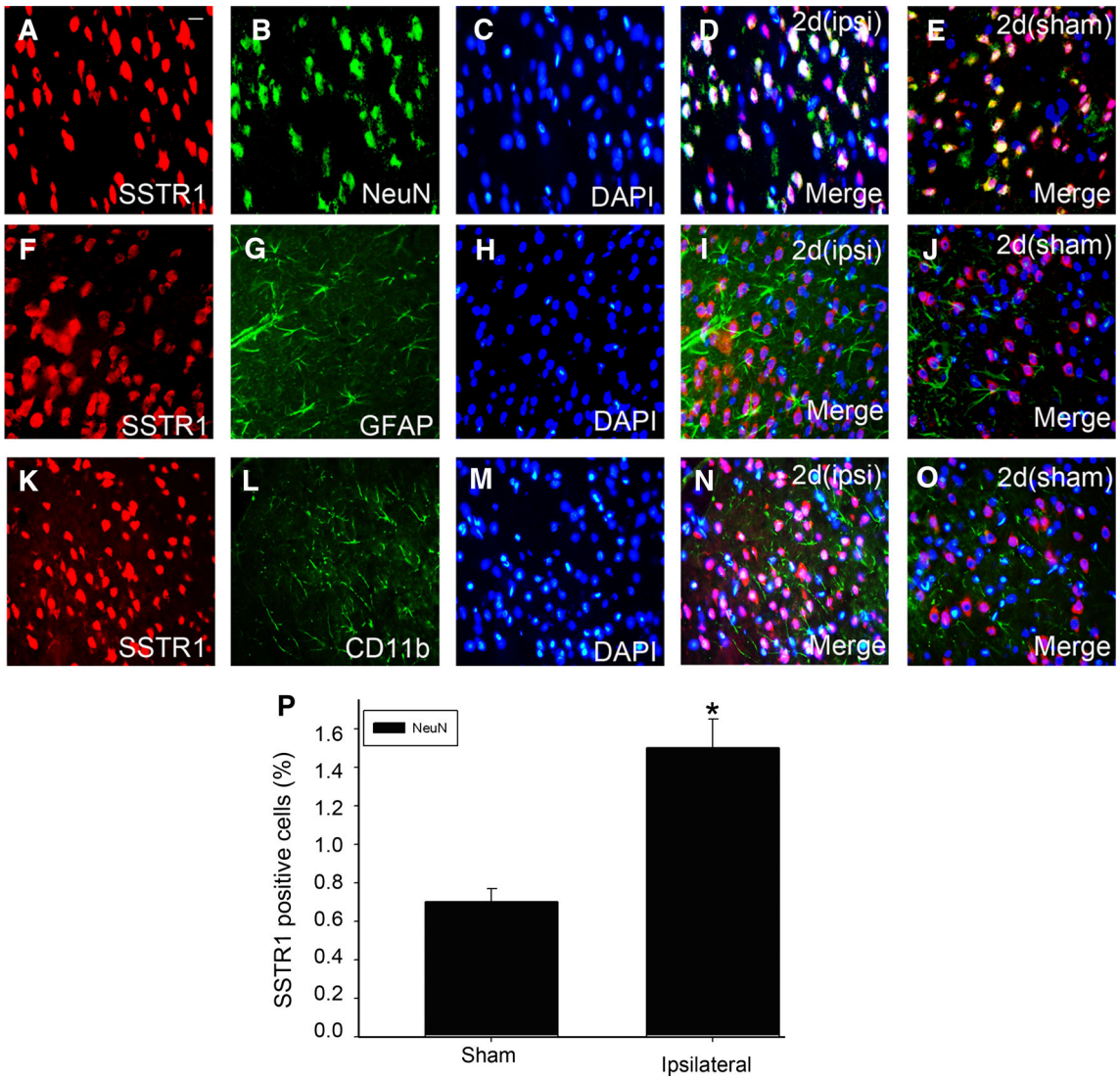

Fig. 3 Colocalization between SSTR1 and different cellular markers by double immunofluorescent staining. In the adult rat caudate within 3 mm distance from the hematoma at the second day after ICH, horizontal sections were labeled with SSTR1 (*Red* **a**, **f**, **k**), different cell markers (*Green* **b**, **g**, **l**) such as neuronal marker (NeuN), astrocyte marker (GFAP) and microglia marker (CD11b). Nuclei were visualized using DAPI (*Blue* **c**, **h**, **m**). The *yellow* and *white* color visualized in the merged images represented the colocalizations between SSTR1 and different phenotype-specific markers (**d**, **e**) and the *purple color* indicated the colocalizations of the nucleus with phenotype-specific markers (**d**, **e**, **i**, **j**, **n**, **o**). Colocalizations between SSTR1 and different phenotype-specific markers in the sham group (**e**, **j**, **o**) were manifested in the caudate. *P* Quantitative analysis of different phenotype-specific markers positive cells expressing SSTR1 (%) in the sham group and 2 day after ICH. The change of SSTR1 expression in the caudate after ICH occurred prominently in neurons. (ipsi) indicates the perihematomal region and (sham) presents the sham group. *Asterisks* indicates significant difference at $p < 0.05$ compared with the sham group. *Error bars* represent SEM. *Scale bars* 20 μm (**a**) (Color figure online)

double immunofluorescence was used to co-localize SSTR2 with different markers, including NeuN (Fig. 3b), GFAP (Fig. 3g), or CD11b (Fig. 3l). We found that SSTR1 was predominantly localized in the nucleus of neurons (Fig. 3a–e), whereas the expression of SSTR1 was barely detected in astrocytes as well as in microglia (Fig. 3f–o). Besides, the number of SSTR1-positive neurons in each mm was counted and found to be significantly elevated in the peri-ICH region, compared with the sham group. We also performed the DAPI labeling in the cell at day 2 after ICH (Fig. 3c, h). These findings were consistent with the results of immunohistochemistry staining, and the localizations of SSTR1 appeared to be confined to the nucleus and cytoplasm of neurons.

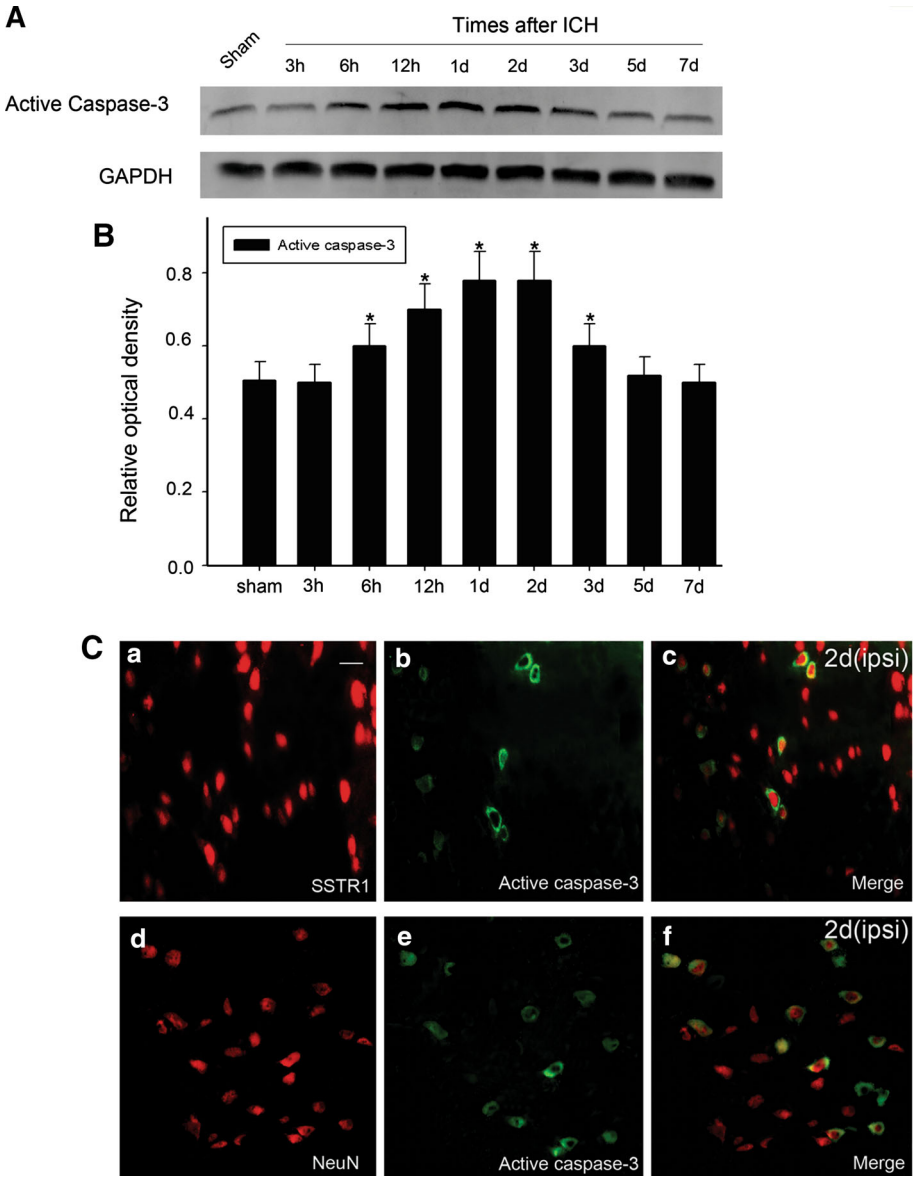

Fig. 4 Association of SSTR1 with neuronal apoptosis after ICH. **a** Western blot analysis of active caspase-3 expression in brain tissues after ICH. The expression of caspase-3 increased after ICH and peaked at 2 days. GAPDH was used to confirm that equal amount of protein was run on gel. **b** Quantification graphs (relative optical density) of the intensity of staining of SSTR1 to GAPDH at each time point. The data are mean ± SEM. ($n = 3$, $^*p < 0.05$, significantly distinct from the normal group and sham group). **c** In brain coronal slices within 3 mm distal to the hematoma, the colocalization between active caspase-3 and SSTR1 were detected. Moreover, there were colocalizations between the active caspase-3 and NeuN (*f*). (ipsi) indicates perihematomal region. *Scale bars* 20 μm (**a**)

Apoptosis After ICH

A previous study suggested that SSTR1 played a part in the regulation of apoptosis apoptosis in retinal pigment epithelium (Papadaki et al. 2010). However, whether SSTR1 was involved in the apoptosis of neuronal cells remains unclear. Therefore, we examined the protein level of active caspase-3 and its colocalizations with SSTR1. The expression of active caspase-3 increased following ICH and peaked at day 1 (Fig. 4a, b). Moreover, the colocalizations of SSTR1/active caspase-3 in addition to active caspase-3/NeuN (Fig. 4c) indicated SSTR1 might participate in neuronal apoptosis after ICH.

In tumor cells, SSTR1 can promote the apoptosis of tumor cells and affect the progression of colorectal cancer by down-regulating the expression of bcl-2. Therefore, we detected the protein level of bcl-2 and its colocalizations with SSTR1 at day 2 after ICH. The expression of bcl-2 was reduced 12 h after ICH and gradually returned to the basal level thereafter (Fig. 5a, b). We also investigated the colocalization of bcl-2 with SSTR1. Double labeling immunofluorescent staining revealed that SSTR1 was colocalized with bcl-2 in the peri-ICH region. Despite that, the colocalizations between bcl-2 and NeuN were also found (Fig. 5c).

SSTR1 Regulates the Expression of Active-Caspase-3 and Neuronal Apoptosis in Vitro

To inspect the role of SSTR1 in neuronal apoptosis, siRNA was used to knock down the expression of SSTR1 in PC12 cells. Cells transfected with SSTR1-siRNA, non-specific

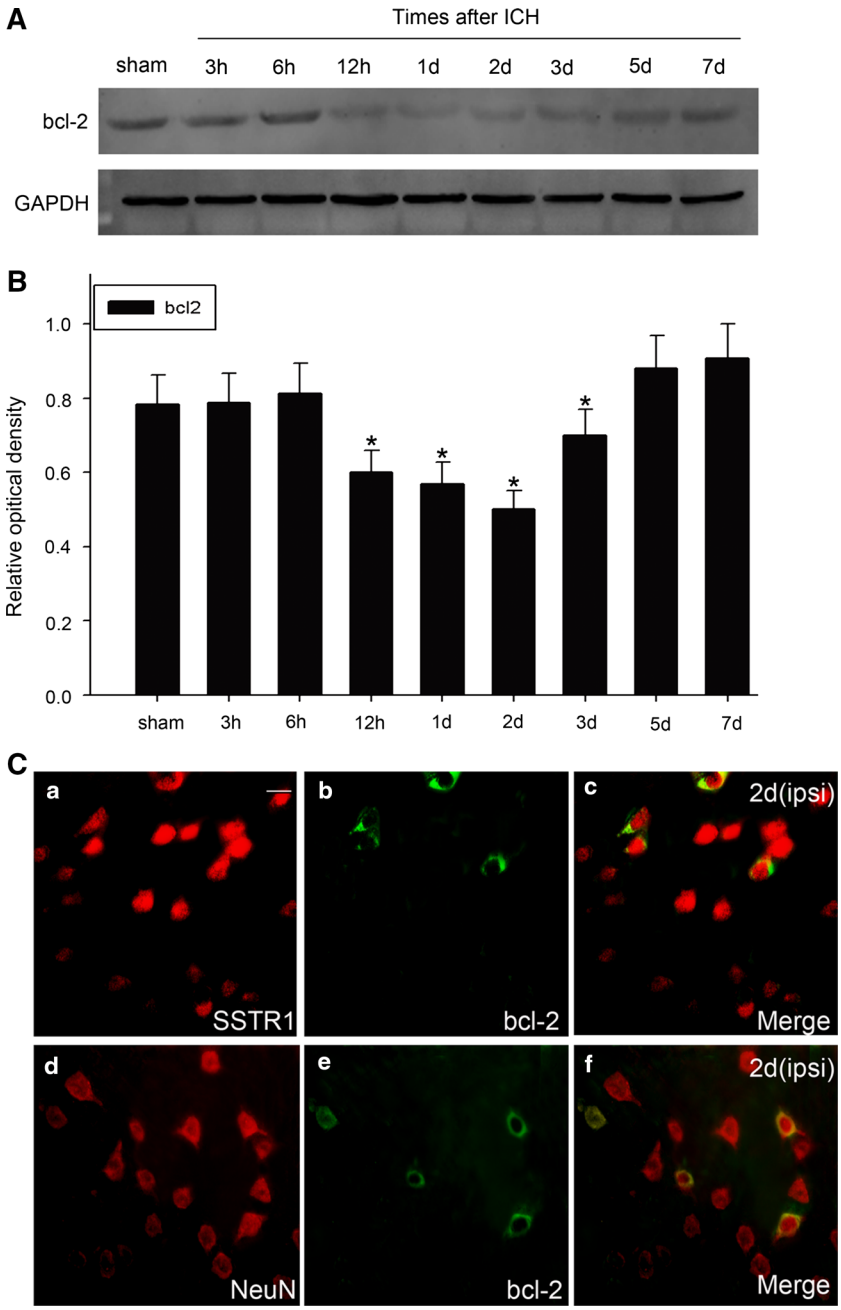

Fig. 5 **a** Detection of the relationship between SSTR1 and bcl-2 after ICH. Western blot analysis of bcl-2 expression in brain tissues after ICH. The expression of bcl-2 decreased after ICH and reached valley at 2 days. **b** Quantification graph (relative optical density) of the intensities of bcl-2 expression to GAPDH at each time point. The data are mean ± SEM ($p < 0.05$, *Asterisks* indicates significantly different from the normal group and sham group). **c** The colocalizations of SSTR1 with NeuN and bcl-2 were also detected by double immunofluorescent staining in the perihematomal region (*c*, *f*). (ipsi) indicates the perihematomal region. *Scale bars* 20 μm (*a*)

siRNA, or vehicle were subjected to Western blot analysis 48 h after transfection. In this way, high interference efficiency of SSTR1-siRNA was confirmed (Fig. 6a, b). The level of active-caspase-3 significantly declined 12 h after SSTR1 silencing in the presence or absence of hemin stimulation (Fig. 6c, d). The result was verified using immunofluorescent staining (Fig. 6e).

Discussion

In the current study, we established a controlled autologous blood injection ICH model in adult rats to mimic the clinical ICH. The rats suffering from ICH exhibited significantly functional deficits, as assessed by behavioral testing. Western blot and immunohistochemistry analyses indicated that SSTR1 was significantly increased at 2 days in regions surrounding the hematoma after ICH. Simultaneously, there was a similar up-regulation of active-caspase-3 with that of SSTR1 in a time-dependant manner. Double immunofluorescence labeling manifested that SSTR1 was only located in neurons, but not in astrocytes or microglia. In addition, colocalizations of SSTR1 and active caspase-3 as well as bcl-2 were detected around the hematoma. Immunohistochemistry and immunofluorescence assays both manifested that

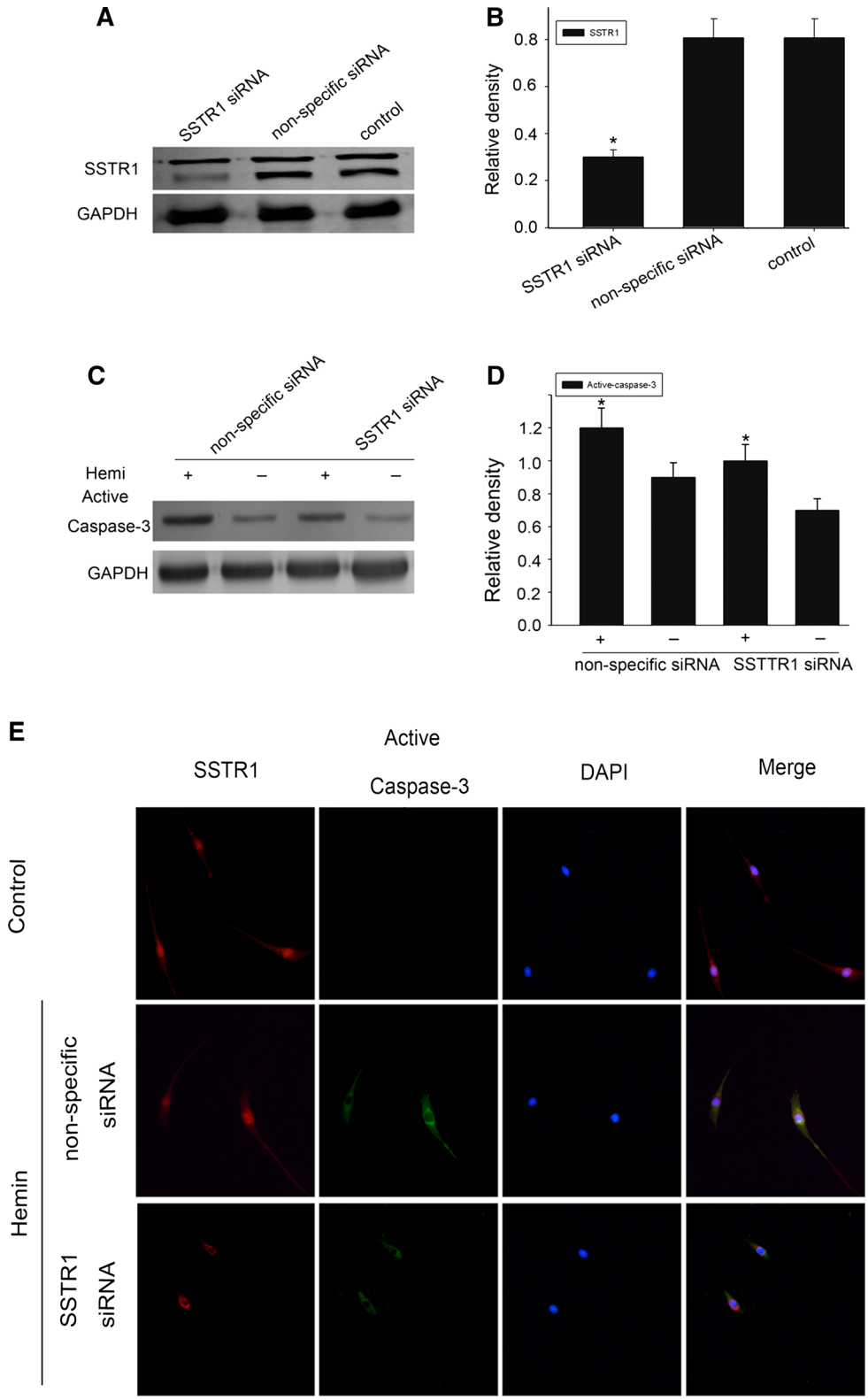

Fig. 6 Involvement of SSTR1 in hemin-induced neuronal apoptosis. Western blot analysis showed the interference efficiency of SSTR1-siRNA oligo in PC12 cells (**a**). Depletion of SSTR1 reduced the level of active-caspase-3 (**c**). The *bar chart* indicated the relative densities of SSTR1 and active-caspase-3 to GAPD H (**b**, **d**). Data are mean ± SEM (*asterisk* means $p < 0.05$, *pound sign* denotes $p < 0.05$). Immunofluorescent analysis of the colocalization between SSTR1 and active-caspase-3 in control, non-specific siRNA or SSTR1-siRNA transfected PC12 cells after hemin treatment (**e**)

SSTR1 was localized in the basal ganglia of brain, suggesting that SSTR1 might take a part in the neuronal apoptosis after ICH. In line with the hypothesis, depletion of SSTR1 by siRNA recedes the apoptosis of PC12 cells, indicating that SSTR1 may play a pro-apoptotic role in nuerons after ICH. All the above data suggest that SSTR1 may facilitate neuronal apoptosis though extrinsic pathway following ICH.

In addition to primary injury, ICH brings about a series of molecular and cellular events (Wang and Dore 2007; Xi et al. 2004). A large amount of previous researches pointed to a critical involvement of neuronal apoptosis in the pathology of ICH. In the current study, neuronal apoptosis and induction of caspase-3 cleavage were investigated adjacent to hematoma in the animals' brains. The secondary injury following ICH contains both anti-apoptotic and pro-apoptotic signaling cascades. Nevertheless, the correlation between SSTR1 expression and neuronal apoptosis suggests that SSTR1 may exert pro-apoptotic function in ICH. In the process of apoptosis after ICH, mitochondria-mediated intrinsic pathway plays an important role. Mitochondria are cellular organelles-where soluble proteins embracing cytochrome c exist and the release of cytochrome c from the intermembrane space into the cytosol could initiate caspase activation (Kroemer et al. 2007; Vaux 2011). The release of these proteins require compromised integrity of the mitochondrial outer membrane (OMM) (Rui et al. 2013). The above process is triggered by the name of OMM permeabilization (MOMP). bcl-2 family proteins are the vital effectors of this process. They oligomerize and imbed in the OMM when spurred by apoptotic signals, then form lipidic pores induce MOMP and the release of cytochrome c, leading to subsequent caspase-3 activation and cell apoptosis (Martinou and Youle 2011). As a critical executor of apoptosis, caspase-3 brings signals together from both the intrinsic and extrinsic pathways.

Neuronal apoptosis exerts vital influence on various CNS diseases, such as ischemia stroke and intracerebral hemorrhage (Broughton et al. 2009), and involves complex and sophisticated pro-apoptotic and anti-apoptotic signals. However, the exact relationship between neuronal apoptosis and SSTR1 remains to be elucidated. Multiples studies have demonstrated that the activation of some SSTR subtypes not only directly inhibited the proliferation of tumor cells, but also was relevant to apoptosis (Qiu et al. 2006; War and Kumar 2012; War et al. 2011). A previous data suggested that Bnip3L might be involved in neuronal apoptosis in ICH through interacting with bcl-2 (Rui et al. 2013). bcl-2 is an apoptosis suppressor and important parameter of apoptosis. The expression of bcl-2 was strikingly decreased in colorectal cancer cells with positive expression of SSTR1, SSTR2, SSTR3, or SSTR5, indicating that the four SSTR subtypes can promote the apoptosis of tumor cells and affect the progression of colorectal cancer by down-regulating the bcl-2 expression or counteracting the anti-apoptosis effects of bcl-2. Apoptosis is mediated by SSTR1 via a block in the G1/S progression in the cell cycle (Qiu et al. 2006; Stetak et al. 2001). However, the molecular mechanism that SSTR1 regulates apoptosis after ICH remains rarely known. This prompts us to question whether SSTR1 is relate to neuroal apoptosis following ICH. SSTR1 was the one of predominant subtypes in all kinds of tissues; also the expression of bcl-2 has correlation with positive expression of SSTR1, 2, 3, 5 in colorectal cancer cells (Qiu et al. 2006). bcl-2 family proteins regulate and contribute to programmed cell death or apoptosis. It is a large protein family and all members contain at least one of four BH domains. Certain members such as bcl-2, bcl-xl, and mcl1 are anti-apoptotic, while others are pro-apoptotic. DNA damage can activate p53, which results in the up-regulation of Bax and down-regulation of bcl-2. The imbalance of Bax/bcl-2 facilitates additional release of cytochrome c. The release of cytochrome c conduces to the activation of caspase-9 and the subsequent activation of caspase-3. A raise of Fas and Fas-L induced the activation of caspase-8 leading to the activation of caspases-3, the latter induces apoptosis (Jiang et al. 2014). Thereby, we studied the expression and distribution of SSTR1 in brain caudate putamen surrounding the hematoma and found that SSTR1 expression was parallel with the expression of active-caspase-3 in both time-dependent and region-specific manners, and there was also partial co-labling between active-caspase-3 and SSTR1 at day 2 after ICH. Our results investigating that knocking down SSTR1 triggers apoptosis in PC12 cells suggest that SSTR1 may play its pro-apoptotic role via the intrinsic pathway.

Our present study demonstrated for the first time that the expression of SSTR1 was markedly increased around the hematoma after ICH, which manifested SSTR1 that might be involved in the physiological and pathological processes following ICH. ICH is a furious and devastating CNS disease with high morbidity and mortality. Therefore, a more clear understanding about the molecular and cellular mechanisms underlying neuronal apoptosis following ICH is in urgent need for the development of improved treatment. Our results supported the hypothesis that up-regulation of SSTR1 around the hematoma was involved in neuronal apoptosis following ICH, probably through the modulation of bcl-2 expression. According approaches targeting SSTR1 activation might elicit beneficial effects in the prevention of deteriorating result after ICH, implying that SSTR1 may serve as a therapeutic target of ICH. Upregulated expression of SSTR1 that is involved in neuronal apoptosis reveals that SSTR1 may be considered as a therapeutic target in ICH. Further studies should be executed to clarify the detailed involvement of SSTR1 in CNS pathology, hereby achieving better prognosis following ICH.

Acknowledgments This work was supported by National Natural Science Foundation of China (No. 81371367, No. 31370803), Natural Science Foundation of Jiangsu Province (No. BK2009156, No. BK2009157, No. BK2009161), Nantong City Social Development Projects Fund (No. HS2012032), Development Fund for Collaborative

Innovation Center of Glycoscience of Shandong University and A Project Funded by the Priority Academic Program Development of Jiangsu Higher Education Institutions (PAPD).

References

Akopian A, Johnson J, Gabriel R, Brecha N, Witkovsky P (2000) Somatostatin modulates voltage-gated K(+) and Ca(2+) currents in rod and cone photoreceptors of the salamander retina. J Neurosci 20:929–936

Aronowski J, Zhao X (2011) Molecular pathophysiology of cerebral hemorrhage: secondary brain injury. Stroke 42:1781–1786

Bradl M, Lassmann H (2010) Oligodendrocytes: biology and pathology. Acta Neuropathol 119:37–53

Broughton BR, Reutens DC, Sobey CG (2009) Apoptotic mechanisms after cerebral ischemia. Stroke 40:e331–e339

Chatterjee S et al (2007) Prolonged somatostatin therapy may cause down-regulation of SSTR-like GPCRs on Schistosoma mansoni. J Vector Borne Dis 44:164–180

Cregan SP, MacLaurin JG, Craig CG, Robertson GS, Nicholson DW, Park DS, Slack RS (1999) Bax-dependent caspase-3 activation is a key determinant in p53-induced apoptosis in neurons. J Neurosci 19:7860–7869

Epelbaum J, Dournaud P, Fodor M, Viollet C (1994) The neurobiology of somatostatin. Crit Rev Neurobiol 8:25–44

Hu C et al (2004) The effect of somatostatin and SSTR3 on proliferation and apoptosis of gastric cancer cells. Cancer Biol Ther 3:726–730

Hua Y, Schallert T, Keep RF, Wu J, Hoff JT, Xi G (2002) Behavioral tests after intracerebral hemorrhage in the rat. Stroke 33:2478–2484

Huan W et al (2012) Spatiotemporal patterns and essential role of TNF receptor-associated factor 5 expression after rat spinal cord Injury. J Mol Histol 43:527–533

Ikram MA, Wieberdink RG, Koudstaal PJ (2012) International epidemiology of intracerebral hemorrhage. Curr Atheroscler Rep 14:300–306

Jiang H, Li J, Zhou T, Wang C, Zhang H, Wang H (2014) Colistin-induced apoptosis in PC12 cells: involvement of the mitochondrial apoptotic and death receptor pathways. Int J Mol Med 33:1298–1304

Karabiyikoglu M, Hua Y, Keep RF, Ennis SR, Xi G (2004) Intracerebral hirudin injection attenuates ischemic damage and neurologic deficits without altering local cerebral blood flow. J Cereb Blood Flow Metab 24:159–166

Karwacki Z et al (2005) Apoptosis in the course of experimental intracerebral haemorrhage in the rat. Folia Morphol (Warsz) 64:248–252

Kroemer G, Galluzzi L, Brenner C (2007) Mitochondrial membrane permeabilization in cell death. Physiol Rev 87:99–163

Li L et al (2013) Up-regulation of NFATc4 involves in neuronal apoptosis following intracerebral hemorrhage. Cell Mol Neurobiol 33:893–905

Liu X, Kim CN, Yang J, Jemmerson R, Wang X (1996) Induction of apoptotic program in cell-free extracts: requirement for dATP and cytochrome c. Cell 86:147–157

Liu X, Yuan D, Nie X, Shen J, Yan Y, Zhang D, Gu J (2014) BTEB2 prevents neuronal apoptosis via promoting bad phosphorylation in rat intracerebral hemorrhage model. J Mol Neurosci

Martinou JC, Youle RJ (2011) Mitochondria in apoptosis: bcl-2 family members and mitochondrial dynamics. Dev Cell 21:92–101

Papadaki T, Tsilimbaris M, Pallikaris I, Thermos K (2010) Somatostatin receptor activation (sst(1) -sst(5)) differentially influences human retinal pigment epithelium cell viability. Acta Ophthalmol 88:e228–e233

Patel YC (1999) Somatostatin and its receptor family. Front Neuroendocrinol 20:157–198

Patel YC, Srikant CB (1994) Subtype selectivity of peptide analogs for all five cloned human somatostatin receptors (hsstr 1-5). Endocrinology 135:2814–2817

Qiu CZ, Wang C, Huang ZX, Zhu SZ, Wu YY, Qiu JL (2006) Relationship between somatostatin receptor subtype expression and clinicopathology, Ki-67, bcl-2 and p53 in colorectal cancer. World J Gastroenterol 12:2011–2015

Qureshi AI, Mendelow AD, Hanley DF (2009) Intracerebral haemorrhage. Lancet 373:1632–1644

Reubi JC (1992) Somatostatin receptors in the gastrointestinal tract in health and disease. Yale J Biol Med 65:493–503 discussion 531-496

Rochaix P et al (1999) Gene therapy for pancreatic carcinoma: local and distant antitumor effects after somatostatin receptor sst2 gene transfer. Hum Gene Ther 10:995–1008

Rui Y et al (2013) Up-regulated expression of Bnip3L after intracerebral hemorrhage in adult rats. J Mol Histol 44:497–505

Sharma K, Srikant CB (1998) G protein coupled receptor signaled apoptosis is associated with activation of a cation insensitive acidic endonuclease and intracellular acidification. Biochem Biophys Res Commun 242:134–140

Sharma K, Patel YC, Srikant CB (1996) Subtype-selective induction of wild-type p53 and apoptosis, but not cell cycle arrest, by human somatostatin receptor 3. Mol Endocrinol 10:1688–1696

Stetak A, Lankenau A, Vantus T, Csermely P, Ullrich A, Keri G (2001) The antitumor somatostatin analogue TT-232 induces cell cycle arrest through PKCdelta and c-Src. Biochem Biophys Res Commun 285:483–488

Teijeiro R, Rios R, Costoya JA, Castro R, Bello JL, Devesa J, Arce VM (2002) Activation of human somatostatin receptor 2 promotes apoptosis through a mechanism that is independent from induction of p53. Cell Physiol Biochem 12:31–38

Tsai CF, Thomas B, Sudlow CL (2013) Epidemiology of stroke and its subtypes in Chinese vs white populations: a systematic review. Neurology 81:264–272

Vaux DL (2011) Apoptogenic factors released from mitochondria. Biochim Biophys Acta 1813:546–550

Wang J, Dore S (2007) Inflammation after intracerebral hemorrhage. J Cereb Blood Flow Metab 27:894–908

War SA, Kumar U (2012) Coexpression of human somatostatin receptor-2 (SSTR2) and SSTR3 modulates antiproliferative signaling and apoptosis. J Mol Signal 7:5

War SA, Somvanshi RK, Kumar U (2011) Somatostatin receptor-3 mediated intracellular signaling and apoptosis is regulated by its cytoplasmic terminal. Biochim Biophys Acta 1813:390–402

Watt HL, Kharmate GD, Kumar U (2009) Somatostatin receptors 1 and 5 heterodimerize with epidermal growth factor receptor: agonist-dependent modulation of the downstream MAPK signalling pathway in breast cancer cells. Cell Signal 21:428–439

Xi G, Fewel ME, Hua Y, Thompson BG Jr, Hoff JT, Keep RF (2004) Intracerebral hemorrhage: pathophysiology and therapy. Neurocrit Care 1:5–18

Xue M, Del Bigio MR (2003) Comparison of brain cell death and inflammatory reaction in three models of intracerebral hemorrhage in adult rats. J Stroke Cerebrovasc Dis 12:152–159

Yoon JH, Lee HH, Yi ES, Baek SG (2013) Age-dependent effect of treadmill exercise on hemorrhage-induced neuronal cell death in rats. J Exerc Rehabil 9:506–510